



Increased global integration in the brain after psilocybin therapy for depression

Richard E. Daws^{1,2}✉, Christopher Timmermann^{1,3}, Bruna Giribaldi³, James D. Sexton^{1,3},
Matthew B. Wall^{4,5,6}, David Erritzoe³, Leor Roseman³, David Nutt^{1,3} and Robin Carhart-Harris^{3,7}

Psilocybin therapy shows antidepressant potential, but its therapeutic actions are not well understood. We assessed the sub-acute impact of psilocybin on brain function in two clinical trials of depression. The first was an open-label trial of orally administered psilocybin (10 mg and 25 mg, 7 d apart) in patients with treatment-resistant depression. Functional magnetic resonance imaging (fMRI) was recorded at baseline and 1 d after the 25-mg dose. Beck's depression inventory was the primary outcome measure (MR/J00460X/1). The second trial was a double-blind phase II randomized controlled trial comparing psilocybin therapy with escitalopram. Patients with major depressive disorder received either 2 × 25 mg oral psilocybin, 3 weeks apart, plus 6 weeks of daily placebo ('psilocybin arm') or 2 × 1 mg oral psilocybin, 3 weeks apart, plus 6 weeks of daily escitalopram (10–20 mg) ('escitalopram arm'). fMRI was recorded at baseline and 3 weeks after the second psilocybin dose (NCT03429075). In both trials, the antidepressant response to psilocybin was rapid, sustained and correlated with decreases in fMRI brain network modularity, implying that psilocybin's antidepressant action may depend on a global increase in brain network integration. Network cartography analyses indicated that 5-HT2A receptor-rich higher-order functional networks became more functionally interconnected and flexible after psilocybin treatment. The antidepressant response to escitalopram was milder and no changes in brain network organization were observed. Consistent efficacy-related brain changes, correlating with robust antidepressant effects across two studies, suggest an antidepressant mechanism for psilocybin therapy: global increases in brain network integration.

Depression is a highly prevalent mental health condition¹, the incidence of which has increased during the COVID-19 pandemic², for example, as reflected in increased prescriptions of antidepressant medications³. However, even the best-performing antidepressant drugs show modest efficacy, non-negligible side effects, discontinuation problems and high relapse rates^{4–7}, highlighting the need for new, improved treatments⁸.

Patients with a diagnosis of depression often exhibit a negative cognitive bias, characterized by pessimism, poor cognitive flexibility, rigid thought patterns and negative fixations regarding 'self' and the future^{9,10}. A number of authors have directly or indirectly taken inspiration from dynamical systems theory to describe depressive episodes as 'attractor states' (stereotyped cognitive states with 'gravitational pull'¹¹).

Neuroimaging research has consistently found examples of abnormal brain functioning in depression, resonant with its phenomenology^{12–14}. A hierarchically supraordinate intrinsic brain network¹⁵, the default mode network (DMN), is associated with introspection and self-referential thinking¹⁶. These cognitive functions are often overactive in depression⁹, and several studies have linked excessive engagement of DMN functioning with depressive symptomatology¹².

In addition to the DMN, other higher-order brain networks such as the executive network (EN) and salience network (SN) have been implicated in depression^{14,17}. These networks are associated with 'cognitive control' and internal versus external attention switching^{18–20}. Such attentional switching is often impaired in depression²¹.

Tellingly, the serotonin 2A (5-HT2A) receptor subtype, which is the key proteomic binding site of 'classic' serotonergic psychedelic drugs, such as psilocybin²², is most densely expressed in a broad pattern of cortex that closely resembles a conjunction map of the DMN, EN and SN²³, corresponding to the transmodal portion of the brain's principal hierarchical gradient¹⁵.

In the last 15 years, at least six separate clinical trials have reported impressive improvements in depressive symptoms with psilocybin therapy²⁴. Included among these studies are (1) an open-label trial in treatment-resistant depression²⁵ and (2) a double-blind, randomized controlled trial (DB-RCT) with an active comparator, the selective serotonin reuptake inhibitor (SSRI) and conventional antidepressant, escitalopram²⁶. These two trials, which included pre-treatment and post-treatment fMRI, are the focus of this paper's analyses.

The therapeutic action of psilocybin and related psychedelics is incompletely understood; however, one model proposes that psychedelics cause a 5-HT2A receptor-induced dysregulation of spontaneous population-level neuronal activity, linked to a temporary 'disintegration' of intrinsic functional brain networks²⁷ and a hypothesized decrease in the precision-weighting of predictive models encoded (at least in part) by the integrity of functional modules²⁸. One important corollary of modular 'disintegration' seems to be the broadening of the brain's functional repertoire of states, commensurate with a broader or flatter global energy landscape²⁹.

Here we hypothesize that the well-replicated finding of brain network disintegration and desegregation under psychedelics^{30,31}

¹The Computational, Cognitive and Clinical Neuroimaging Laboratory (C3NL), Imperial College London, London, UK. ²Centre for Neuroimaging Sciences, Kings College London, London, UK. ³Centre for Psychedelic Research, Division of Academic Psychiatry, Imperial College London, London, UK. ⁴Invicro London, Hammersmith Hospital, London, UK. ⁵Department of Metabolism, Digestion and Reproduction, Faculty of Medicine, Imperial College London, London, UK. ⁶Clinical Psychopharmacology Unit, University College London, London, UK. ⁷Psychedelics Division, Neuroscape, Department of Neurology, University of California, San Francisco, CA, USA. ✉e-mail: richard.daws@kcl.ac.uk

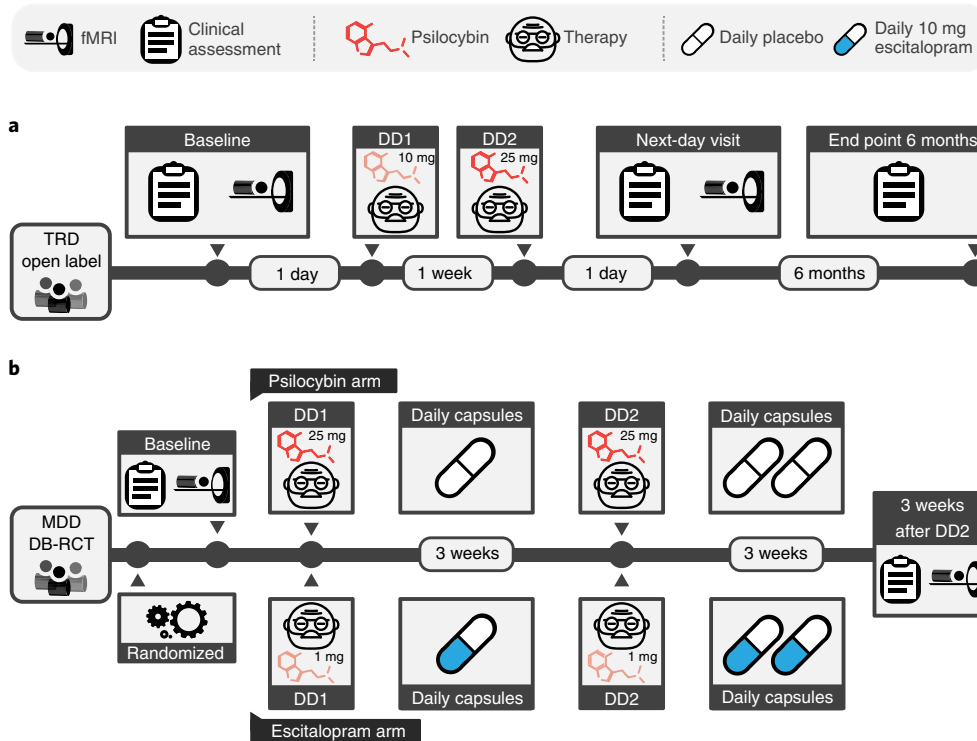


Fig. 1 | Trial design schematics. a, Open-label trial. Eligible patients attended a baseline clinical assessment and resting-state fMRI visit. This was followed by two orally administered psilocybin therapy DDs separated by 1 week, which differed in dose strength (10 mg on DD1, 25 mg on DD2). The post-treatment fMRI scan occurred 1 d after DD2. Remote clinical assessment continued for 6 months. **b**, DB-RCT. Patients attended a baseline clinical assessment and resting-state fMRI visit and were randomly assigned to the psilocybin arm (top) or escitalopram arm (bottom). The psilocybin arm involved 2 × 25 mg psilocybin therapy DDs with 3 weeks of daily placebo capsules following each DD. The escitalopram arm involved 2 × 1 mg psilocybin therapy DDs with 3 weeks of 10 mg daily escitalopram following DD1 and 20 mg of escitalopram following DD2. Both groups attended a post-treatment clinical assessment and fMRI visit 3 weeks and 1 d after DD2.

will be apparent subacutely, in post-treatment resting-state fMRI data. We also hypothesize that this effect, consistent with a flatter energy landscape, will relate to improved depression outcomes and will not be observed after a course of the SSRI, escitalopram.

Results

Open-label trial. Rapid antidepressant effect of psilocybin therapy.

Patients with treatment-resistant depression (TRD) participated in a single-arm, open-label psilocybin therapy clinical trial (Fig. 1a). Baseline clinical assessment and resting-state fMRI were followed by fixed-order ‘low’ (10 mg) and ‘high’ (25 mg) psilocybin therapy dosing days (DDs) that were separated by 1 week. A second clinical assessment and fMRI scan were conducted 1 d after DD2. Remote assessments of clinical status were conducted 1 week, 3 months and 6 months after DD2. Further details are available in Methods and elsewhere²⁵.

Of the 19 patients recruited, 3 were excluded due to excessive fMRI head motion (Fig. 2a). We first confirmed an antidepressant effect of psilocybin in this imaging sample of 16 patients (mean age, 42.75 years, s.d. = 10.15, 4 females) using the Beck Depression Inventory (BDI-1A). This patient-rated measure was preregistered for the original investigation (gtr.ukri.org MR/J00460X/1). The BDI captures a broad range of symptoms and places particular emphasis on the cognitive features of depression³², which may be an important target of psilocybin therapy.

Baseline BDI scores indicated severe depression (mean BDI = 34.81, s.d. = 7.38). In line with our previous report²⁵, rapid, substantial and sustained reductions in depression severity were

observed after treatment (Fig. 3a,b). Relative to baseline, significant BDI reductions were observed at 1 week (mean difference, −21.0 points; $t_{15} = 7.11$, 95% confidence interval (CI) −27.30 to −14.71, $P < 0.001$, Cohen’s $d = 1.78$) and still evident at 6 months (mean difference, −14.19 points; $t_{15} = 4.26$, 95% CI −21.29 to −7.09, $P < 0.001$, $d = 1.07$).

Decreased brain modularity one day after psilocybin therapy.

To test our primary hypothesis, preprocessed fMRI data were used to estimate normalized network modularity from Pearson correlation functional connectivity matrices of the cortex (Methods). Confirming our primary hypothesis, brain network modularity was significantly reduced (Fig. 4a) 1 d after psilocybin therapy (mean difference, −0.29; $t_{15} = 2.87$, 95% CI 0.07 to 0.50, $P = 0.012$, $d = 0.72$). This result implies a global increase in functional connectivity between the brain’s main intrinsic networks.

Decreased modularity predicts improved clinical outcomes.

We hypothesized that decreased brain network modularity would relate to the sustained improvements in depression severity that follow psilocybin therapy. To test this, we calculated Pearson correlations between the post-treatment brain modularity and BDI scores from the three post-treatment time points (1 week, 3 months, 6 months). After false discovery rate (FDR) correction for multiple comparisons, a strong significant Pearson correlation was observed at the 6 months primary end point ($r_{14} = 0.64$, 95% CI 0.29 to 0.84, $P = 0.023$; Fig. 4b). Directionally consistent relationships were seen at 3 months ($r_{14} = 0.46$, 95% CI 0.03 to 0.74, $P = 0.114$) and 1 week

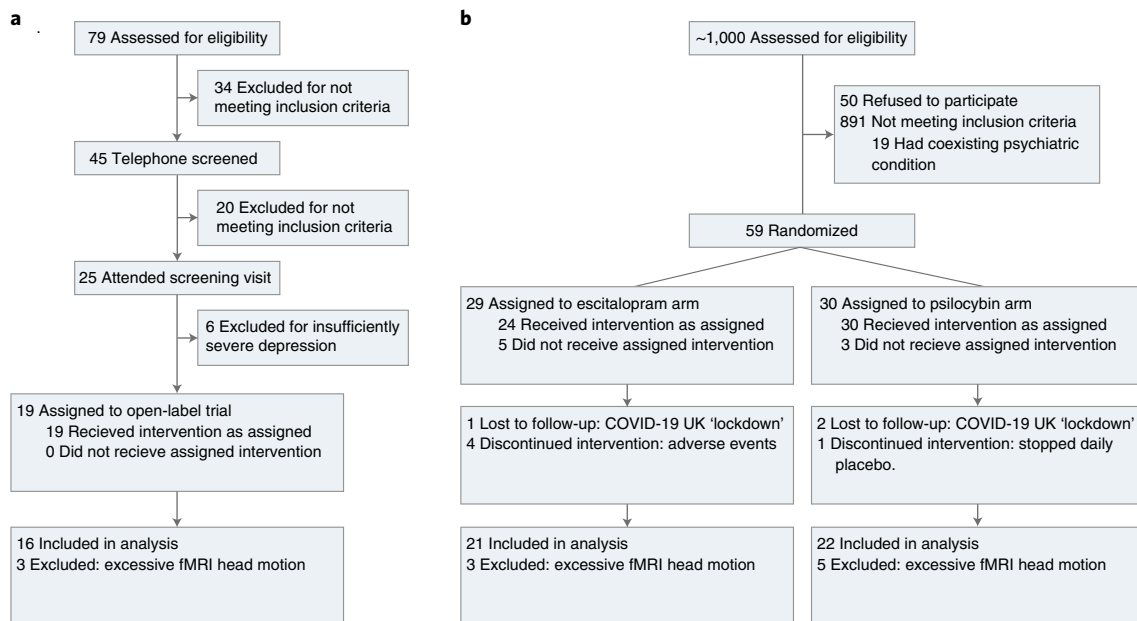


Fig. 2 | Recruitment flow diagrams. a, The open-label trial was conducted during 2015–2016. **b**, The DB-RCT was conducted during 2019–2020.

($r_{14}=0.29$, 95% CI -0.16 to 0.64 , $P=0.284$), but these did not survive correction. Pre-treatment versus post-treatment changes in modularity significantly correlated with change in BDI score at 6 months, relative to baseline ($r_{14}=0.54$, 95% CI 0.14 to 0.78 , $P=0.033$; Fig. 4c). These results imply that decreased brain modularity 1 d after psilocybin therapy relates to long-term improvements in depression symptom severity.

DMN changes in within-network and between-network functional connectivity one day after treatment. Previous research has implicated depressive symptomology with hyperconnectivity of the DMN¹² and hypoconnectivity of the DMN with other higher-order ‘cognitive’ networks, including the EN and SN^{14,17}. We therefore tested for evidence of these abnormalities being attenuated after treatment using functional cartography (Methods). Consistent with our previous hypothesis, significant reductions in DMN network recruitment (mean difference, -0.54 ; $t_{15}=-2.99$, 95% CI -0.92 to -0.15 , $P=0.009$, $d=0.75$; Fig. 4d) and increased between-network integration between the DMN and EN (mean difference, 0.53 ; $t_{15}=3.01$, 95% CI 0.15 to 0.90 , $P=0.01$, $d=0.75$) and between the DMN and SN (mean difference, 0.55 ; $t_{15}=2.89$, 95% CI 0.14 to 0.95 , $P=0.01$, $d=0.72$; FDR-corrected) were observed 1 d after psilocybin therapy. An exploratory analysis of the changes in network recruitment and between-network integration of other brain networks is available in Supplementary Fig. 2.

Taken together, these findings indicate a clinically relevant decrease in brain network modularity following psilocybin therapy for TRD. A network cartography analysis suggests that this global change in network organization may be underpinned by a specific decrease in within-DMN connectivity and increase in DMN connectivity with other higher-order networks, including the EN and SN.

Double-blind randomized controlled trial. Psilocybin therapy versus escitalopram for depression. The design of this DB-RCT (Fig. 1b) gave a new opportunity to compare not just the safety and efficacy, but also the mechanisms of action of psilocybin therapy to those of a conventional antidepressant drug, escitalopram. Patients with major depressive disorder (MDD) were randomly allocated to a ‘psilocybin arm’ or ‘escitalopram arm’ (Fig. 1b). Baseline clinical

assessment and resting-state fMRI was followed by DD1, when patients received either 25 mg psilocybin (psilocybin arm) or a presumed inactive 1 mg psilocybin dose (escitalopram arm). All patients were informed that they would receive psilocybin but were blind to the dosage. DD2 occurred 3 weeks after DD1 and was a duplicate dosage. Beginning 1 d after DD1, patients took daily capsules for 6 weeks and 1 d in total. For both conditions, one capsule per day was ingested for the first 3 weeks and two capsules per day were ingested thereafter. Capsule content was either inert placebo (microcrystalline cellulose in the psilocybin arm) or 10 mg escitalopram in the escitalopram arm (10 mg daily for the first 3 weeks and 2×10 mg (20 mg) daily for the final 22 d). Further details are available in Methods and elsewhere²⁶.

Of the 59 patients with MDD recruited, 29 were randomly allocated to the escitalopram arm. Of those, four discontinued due to adverse reactions to escitalopram, one was lost due to the COVID-19 UK lockdown and three were excluded due to excessive fMRI head motion (Fig. 2b). The remaining 21 patients (mean age, 40.9 years, s.d. = 10.1, 6 female) were included in the escitalopram imaging sample. Thirty patients were randomly allocated to the psilocybin arm. Of those, one was excluded for choosing not to take the daily (placebo) capsules, two did not attend the post-treatment session due to the COVID-19 UK lockdown and five were excluded due to excessive fMRI head motion. The remaining 22 patients (mean age, 44.5 years, s.d. = 11.0, 8 female) were included in the psilocybin imaging sample (Fig. 2b).

The BDI was a primary outcome measure for the open-label trial (MR/J00440/1) and a secondary outcome measure for this DB-RCT (ClinicalTrials.gov identifier NCT03429075); however, this measure proved to be an especially sensitive index of post-psilocybin reductions in symptom severity across the trials²⁶. Between trials, baseline BDI (Fig. 3c) was significantly greater in the open-label TRD trial compared with the DB-RCT MDD trial (mean difference, 6.53 points; $t_{57}=3.01$, 95% CI 2.18 to 10.88 , $P=.013$, $d=0.83$). This difference is likely due to TRD being an inclusion criteria in the open-label trial, but not in this DB-RCT.

As described in our previous report²⁶, BDI-measured reductions in depressive symptom severity were significantly greater after psilocybin than escitalopram, indicating superior efficacy of psilocybin therapy versus escitalopram (Fig. 3d). Moreover, we confirmed

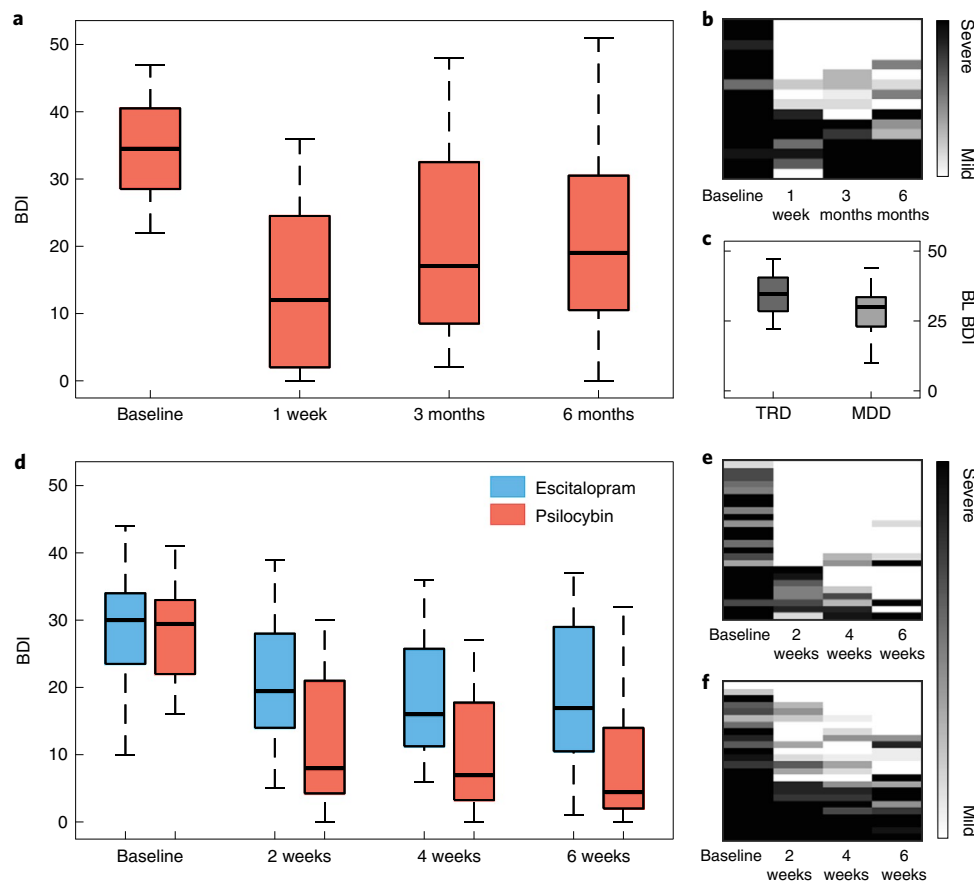


Fig. 3 | Beck depression inventory scores. **a**, Open-label trial box plots of BDI scores of patients with TRD across time points. **b**, Qualitative raster plots of individual patient's BDI score for each time point (columns). **c**, Baseline BDI of patients with TRD in the open-label trial was significantly greater than that in patients with MDD in the DB-RCT ($t_{57}=3.01$, 95% CI 2.18 to 10.88, $P=0.013$, $d=0.83$). **d**, DB-RCT BDI scores from each study arm and time point. **e,f**, Qualitative raster plots of individual patient's BDI for each time point for the psilocybin arm (**e**) and escitalopram arm (**f**). The box plot central marks represent the group median, the box edges represent the 25th to 75th percentiles and the whiskers extend to the data range. Independent samples of $n=16$ TRD were used in **a** and alongside $n=43$ MDD in **c**, of which $n=21$ in the escitalopram arm and $n=22$ in the psilocybin arm are displayed in **d**. The rows from each qualitative raster plot were ordered by the sum BDI score across time points.

the statistical significance of this contrast within the smaller neuroimaging sample included in the present analyses after testing for an arm \times time point analysis of variance interaction on BDI scores ($F_{3,123}, 4.47$; $P=0.005$). FDR-corrected pairwise comparisons relative to baseline were significantly different at 2 weeks (mean difference, -8.73 ; $t_{41}=-3.66$, 95% CI -13.55 to -3.91 , $P=0.002$, $d=0.98$), 4 weeks (mean difference, -7.79 ; $t_{41}=-2.69$, 95% CI -13.62 to -1.95 , $P=0.013$, $d=0.77$) and at 6 weeks (mean difference, -8.78 ; $t_{41}=-2.61$, 95% CI -15.58 to -1.97 , $P=0.013$, $d=0.75$), all favoring the psilocybin arm.

Decreased brain modularity for psilocybin but not escitalopram. Reconfirming our primary hypothesis (Fig. 5a,b) and replicating analyses on the open-label trial data, brain network modularity was significantly reduced at the trial's primary end point, 3 weeks after psilocybin therapy (mean difference, -0.39 ; $t_{21}=-2.20$, 95% CI -0.75 to -0.02 , $P=0.039$, $d=0.47$). Moreover, for the psilocybin condition, post-treatment decreases in brain network modularity significantly correlated with improvements in depression symptom severity at this primary end point ($r_{20}=0.42$, $P=0.025$, one-tailed).

Notably, there was no significant interaction between treatment arm and scanning session on network modularity ($F_{1,41}=2.719$, $P=0.107$); however, there was evidence that the reduction in network modularity and its relationship to depression severity may be specific to the psilocybin arm. Namely, in the escitalopram group

(Fig. 5d,e), network modularity did not change from baseline (mean difference, 0.01; $t_{20}=0.07$, 95% CI -0.35 to 0.33, $P=0.95$, $d=0.02$) and there was no significant correlation between changes in modularity and changes in BDI scores ($r_{19}=0.08$; $P=0.361$, one-tailed).

Response to psilocybin correlates with network flexibility. The specific changes in network recruitment observed 1 d after psilocybin therapy in the open-label trial were not replicated at 3 weeks in this DB-RCT (Supplementary Information). However, the faster fMRI scanning protocol adopted in the DB-RCT generated twice as much temporal data per scanning session (Methods). This provided the rare opportunity to examine changes in the dynamic flexibility of brain networks following psilocybin therapy.

The metric known as 'dynamic flexibility' indexes how often brain regions change their community allegiance over time, during the course of an fMRI scan^{33,34} (Methods). Reduced functional dynamics have been previously associated with depression symptomology¹⁴. In an exploratory analysis, post-psilocybin therapy changes in network flexibility were correlated with changes in BDI score (Fig. 5c). After FDR correction, increased EN dynamic flexibility strongly correlated with greater symptom improvement at the 6-week primary end point for the psilocybin arm ($r_{20}=-0.76$, 95% CI -0.90 to -0.50 , $P=0.001$). Strong correlations that survived FDR correction were also observed when combining regions from the EN with other lateral frontoparietal networks, such as the SN

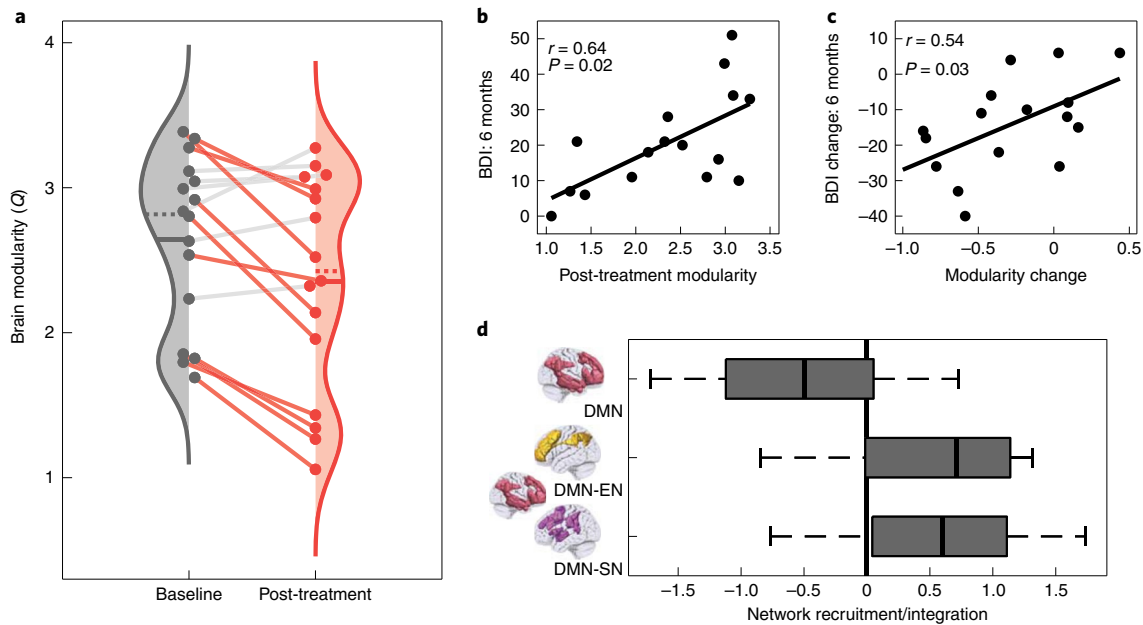


Fig. 4 | Responses of patients with TRD to psilocybin therapy relate to increases in brain network integration. **a**, Brain modularity (normalized Q) significantly reduced, indicating a global increase in brain network integration following psilocybin therapy in patients with TRD ($t_{15} = 2.87$, 95% CI 0.07 to 0.50, $P = 0.012$, $d = 0.72$). The solid and dotted lines represent the mean and median, respectively. Patient's data are connected by solid lines and rendered in color if modularity decreased. **b**, Absolute post-treatment scan modularity correlated with absolute BDI scores at the 6 months primary end point ($r_{14} = 0.64$, 95% CI 0.29 to 0.84, $P = 0.023$, FDR-corrected). **c**, Post-treatment change in brain modularity significantly correlated with treatment response (BDI, baseline – 6 months) ($r_{14} = 0.54$, 95% CI 0.14 to 0.78, $P = 0.033$). **d**, DMN (red) recruitment decreased ($t_{15} = -2.99$, 95% CI -0.92 to -0.15 , $P = 0.009$, $d = 0.75$) and its between-network integration with the EN (gold) ($t_{15} = 3.01$, 95% CI 0.15 to 0.90, $P = 0.01$, $d = 0.75$) and SN (purple) ($t_{15} = 2.89$, 95% CI 0.14 to 0.95, $P = 0.01$, $d = 0.72$) increased following psilocybin therapy (all FDR-corrected). The box plot central marks represent the group median, the box edges represent the 25th to 75th percentiles and the whiskers extend to the data range. Independent samples of $n = 16$ TRD were used in **a–d**.

and dorsal attention network (Fig. 5c). Critically, there were no significant correlations between changes in BDI scores and changes in dynamic flexibility in the escitalopram arm (Fig. 5f).

Discussion

In light of growing evidence for the antidepressant efficacy of psilocybin therapy²⁶, the present findings advance our understanding of its possible underlying brain mechanisms. Across two trials, decreased brain modularity was observed and correlated with improvements in depressive symptomatology. Moreover, this antidepressant action may be specific to psilocybin therapy, as no changes in modularity were observed with the conventional SSRI antidepressant, escitalopram.

Research into the acute brain action of psychedelics has revealed well-replicated changes in global brain function that are somewhat consistent with those observed here (an increased repertoire of inter-regional and between-network functional connectivity (FC)^{29–31}). A previous analysis of ours had suggested some contrasting changes in the architecture of spontaneous brain function 1 d following psilocybin treatment for depression relative to what has been observed during the acute psychedelic state itself: spatially expanded DMN FC (1 d after treatment for TRD) versus acute DMN ‘disintegration’²⁵. However, others have reported evidence of increased inter-network FC 1 week and 1 month after psilocybin treatment³⁵, as well as 1 d after ayahuasca, including increases in DMN-SN FC in healthy volunteers³⁶. These findings are consistent with the present study, but here we show robust and reliable evidence that increases to global brain network integration accompanies the antidepressant efficacy of psilocybin therapy.

The present modularity metrics may be more sensitive indices of the antidepressant action of psilocybin than previously applied

time-averaged within-network and between-network FC analyses²⁵. Indeed, they may bear relevance to other FC metrics applied to acute-state psychedelic fMRI data^{29,30} where a general picture of increased global FC and a broadened dynamic state space has emerged²⁸. In this context, the results could be understood as a ‘carry-over’ effect resembling brain dynamics associated with the acute action of psychedelics, albeit at an attenuated level and in a specific population (depressed patients). To show robustness to analytical method, we also carried out more traditional mass-univariate analyses and these yielded consistent findings (Supplementary Figs. 3 and 4). However, an advantage of network modularity is its capacity to elegantly summarize global changes in the brain's functional network organization³⁷.

Previous research on resting-state activity in depression has found heightened network modularity correlating with symptom severity^{17,38}. Additional work implies heightened within-DMN FC and elevated FC between limbic regions such as the amygdala, and high-level cortical regions correlates with ruminative symptoms in depression^{12,39}. Taken together, a model emerges of abnormally modular spontaneous brain function in depression that is effectively remediated by psilocybin therapy. According to various findings, the FC energy landscape or state space in depression can be described as abnormally constricted, paralleling the narrow, internally focused, ruminative quality of mood and cognition in the disorder¹¹. In contrast, psilocybin seems to increase the brain's ability to visit a broader state space, both acutely and after psilocybin therapy in patients who are depressed, as shown here. Moreover, this ‘liberating’ action of psilocybin is paralleled by subjective reports of ‘emotional release’^{40,41} as well as subacute increases in behavioral optimism⁹, cognitive flexibility⁴² and psychological flexibility after taking a psychedelic drug⁴³. Indeed, heightened emotional responsiveness may be specific to psilocybin therapy versus SSRIs²⁶.

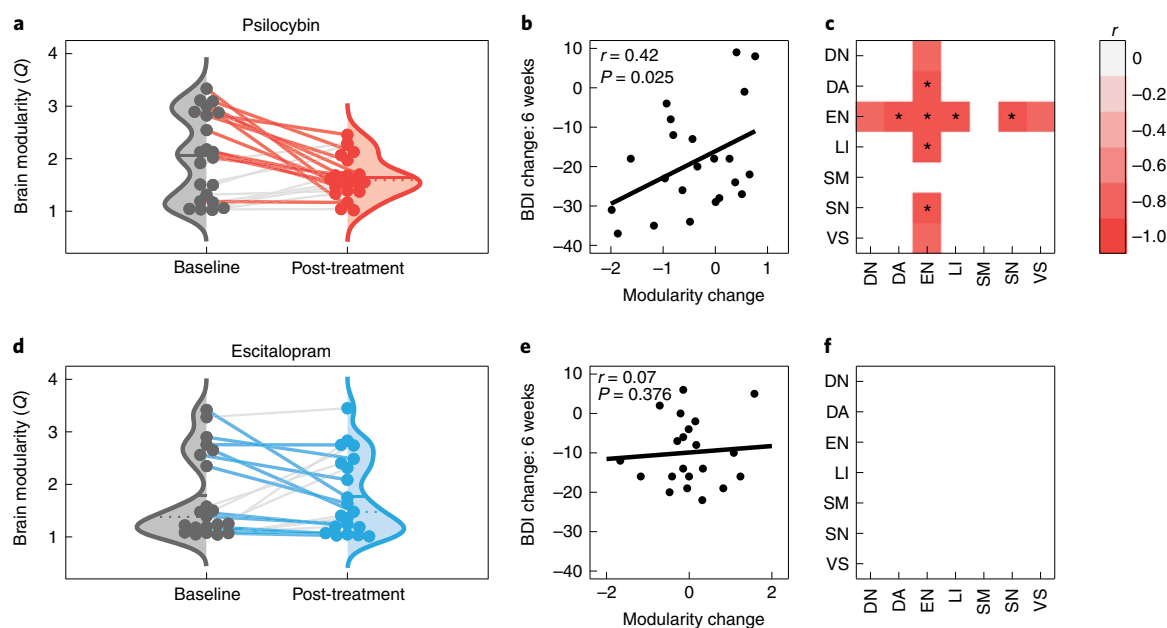


Fig. 5 | Increased global brain network integration correlates with treatment response following psilocybin, but not following escitalopram. **a**, Significant decreases in brain network modularity (normalized Q), indicating greater brain network integration following psilocybin therapy ($t_{21} = -2.20$, 95% CI -0.75 to -0.02 , $P = 0.039$, $d = 0.47$). The solid and dotted lines on the distributions represent the mean and median, respectively. Individual patient data are represented and connected with solid lines between sessions that are rendered with color if modularity decreased between sessions. **b**, Post-treatment change in brain modularity significantly correlated with the treatment response primary end point (BDI, baseline – 6 weeks) ($r_{20} = 0.42$, $P = 0.025$, one-tailed). **c**, Significant correlations between increased dynamic network flexibility and the psilocybin primary end point treatment response (BDI, baseline – 6 weeks) are colored (white, $P > 0.05$; *survives FDR correction). The EN exhibited the largest correlation ($r_{20} = -0.76$, 95% CI -0.90 to -0.50 , $P = 0.001$). **d–f**, The equivalent analyses of brain network modularity in the escitalopram arm did not show significant session differences (**d**), relationship to individual treatment response (**e**) or network flexibility (**f**). $n = 22$ independent psilocybin arm samples are displayed in **a–c** and $n = 21$ independent escitalopram arm samples are displayed in **d–f**. DN, default mode network; DA, dorsal attention; EN, executive network; LI, limbic; SM, somatomotor; SN, salience network; VS, visual.

It is plausible that this putative liberating effect of psilocybin on cortical activity occurs via its direct agonist action on cortical 5-HT_{2A} receptors, dysregulating activity in regions rich in their expression. We surmise that chronic escitalopram does not have the same effect on brain modularity due to its more generalized action on the serotonin system and predominant action on inhibitory postsynaptic 5-HT_{1A} receptors, which are richly expressed in limbic circuitry^{27,44}.

Beyond the global decrease in network modularity after psilocybin, we observed functional changes in DMN, EN and SN dynamics that are consistent with neurobiological models of depression¹⁵. These high-order transmodal networks house the highest density of 5-HT_{2A} receptors, the principal action site for serotonergic psychedelics^{22,23}. Higher-order networks are implicated in the acute action of psychedelics, where they show reduced modularity and increased communication with regions ordinarily outside of their community limits^{29–31}.

The EN and SN have been associated with tasks requiring cognitive flexibility such as learning and task switching^{18,19,46,47}; impaired functioning of these networks have been reported in depression^{14,17} and other disorders exhibiting cognitive inflexibility such as autism spectrum disorder⁴⁸ and obsessive-compulsive disorder⁴⁹. Our results suggest that decreased modularity or increased flexibility of these networks following psilocybin therapy is a key component of its therapeutic mechanism of action. We did not formally assess cognitive flexibility in the clinical trials reported here but we did observe improvements in general cognitive functioning after psilocybin treatment in the DB-RCT, as well as treatment-specific improvements in ‘emotional avoidance’ (an inversion of the related construct ‘psychological flexibility’²⁶).

It should be noted that psychological processes that do not reliably relate to brain modularity changes may have played a role in the main clinical outcomes of this study, and an inability to discount such factors precludes the making of confident inferences that drug alone was the main causal determinant of the imaging outcomes or, indeed, that decreased modularity is sufficient for response to psilocybin therapy. Nevertheless, the changes observed in the neuroimaging data were consistent with previous brain imaging research regarding the acute action of psychedelics and are plausible in light of evidence of elevated modularity and abnormal functioning of higher-order networks in depression^{12,17,38,39,50}.

Successful phase III DB-RCTs will be required to achieve licensing for psilocybin therapy, but pragmatic trials may better address questions regarding treatment practicability, specificity and optimization⁵¹. Given the emerging research into psychedelic therapy, it is important for large-scale trials to establish the generalizability, reliability and specificity of psilocybin’s antidepressant response. For example, it is likely that efficacy will depend on symptom severity, depression subtypes and comorbidities, as well as other key pharmacological and extrapharmacological factors⁵². For brain imaging studies, we would recommend network modularity analyses such as those employed here. fMRI datasets are complex, burdensome and susceptible to noise, contributing to the challenge of detecting reliable biomarkers. Simplifying composite measures, such as network modularity, combined with a research domain, symptoms-based approach to psychological phenomena, may be a particularly productive way forward^{37,51}.

It should be noted that the present study’s findings do not support baseline modularity as a predictor of response to psilocybin therapy. Patients with a range of baseline modularity values showed

modularity reductions after treatment with psilocybin; however, the present results do suggest that the early-phase modularity change is predictive of the long-term treatment response to psilocybin therapy.

It is noteworthy to consider the potentially confounding effects of head motion when interpreting fMRI data. Here, a robust fMRI preprocessing pipeline was employed alongside strict head motion criteria for patient inclusion. To examine robustness to motion, an analysis of head motion was conducted and is available in the Supplementary Information. These analyses bolster the present findings, as there was no evidence that head motion differed between sessions or treatment arms or that it correlated with network modularity. The fMRI data were collected with an eyes-closed protocol, which has some advantages; however, it would be compelling if these findings were replicated in data acquired with an eyes-open protocol. In-scanner sleep can be more likely during eyes-closed fMRI, which is a particular disadvantage⁵³. In-scanner sleep cannot be ruled out here. However, the head motion analyses make it unlikely that sleep was a confounding factor. Furthermore, a self-reported visual analog scale of time spent asleep and ‘sleepiness’ were acquired immediately after all scan runs in study 2. An analysis of these data is available in the Supplementary Information. Critically, ratings of in-scanner sleep or sleepiness were low and did not differ between treatment arms or scanning session.

This study’s primary hypothesis was confirmed and replicated despite substantial differences between the design of the two trials. Baseline depression severity was significantly greater in the open-label trial. Furthermore, the open-label trial post-treatment fMRI scan was only 1 d after DD2 and was recorded with a 12-channel head coil and a 2-s repetition time (TR). In contrast, the DB-RCT post-treatment scan was conducted 3 weeks after DD2 and was recorded with a 32-channel head coil and a 1.25-s TR.

Acknowledging these differences between the trial designs serves to strengthen the validity of the main findings, as they were robustly replicated; however, the lack of replication in the finer-grained cartography analyses limits the network-specific inferences. A supplementary analysis (Supplementary Information) did confirm that baseline depression severity correlated with within-DMN connectivity and between-network DMN-EN and DMN-SN connectivity, as has been previously reported^{12,17,38,39,50}; however, in the DB-RCT, we did not replicate the entirety of the changes in network cartography that were observed in the open-label trial. Given that the observed network effects directly follow predictions from the depression literature, it may be that they are more pronounced in more severe cases, such as those included in the open-label TRD trial. Alternatively, it may be that these effects are only detectable in a short-term, subacute phase after psilocybin therapy and not, for example, 3 weeks later. Parsing the relative contribution of baseline severity and time since treatment will be an important feature of future clinical trials with neuroimaging, ideally with larger samples and repeated scanning sessions.

Dynamic analyses can be challenging to conduct. To be sufficiently powered, time series need to be of sufficient length to be split into multiple time windows that are themselves sufficiently long to compute reliable FC measures, and previous research guided our selection of parameters^{54,55}. Collecting sufficient fMRI data in patient cohorts can be challenging, but given the appeal of dynamic analyses, efforts are underway to facilitate and improve them⁵⁴. It should be noted that a sufficiently broad window of time was used to estimate Pearson correlation FC; however, ongoing work is required to better understand how to capture the most functionally meaningful dynamic data.

With these caveats entered, it should be emphasized that the inferences from both cartography analyses converged on the brain’s higher-order networks. In particular, the DB-RCT analyses showed robust correlations ($r \sim 0.8$) between increased higher-order network

flexibility and psilocybin’s treatment response, and this converges with the open-label trial as well as previous research¹⁴.

In summary, depression is a major public health problem associated with huge burden and cost. Here, we identify a robust, reliable and potentially specific biomarker of response to psilocybin therapy for depression. Our results may help to explain why psilocybin therapy holds promise as a new treatment option in psychiatry.

Online content

Any methods, additional references, Nature Research reporting summaries, source data, extended data, supplementary information, acknowledgements, peer review information; details of author contributions and competing interests; and statements of data and code availability are available at <https://doi.org/10.1038/s41591-022-01744-z>.

Received: 10 May 2021; Accepted: 14 February 2022;

Published online: 11 April 2022

References

1. *Depression and Other Common Mental Disorders: Global Health Estimates* (World Health Organization, 2017).
2. Tang, F. et al. COVID-19 related depression and anxiety among quarantined respondents. *Psychol. Health* **36**, 164–178 (2021).
3. Rabeea, S. A., Merchant, H. A., Khan, M. U., Kow, C. S. & Hasan, S. S. Surging trends in prescriptions and costs of antidepressants in England amid COVID-19. *DARU J. Pharm. Sci.* <https://doi.org/10.1007/s40199-021-00390-z> (2021).
4. Hofmann, S. G., Curtiss, J., Carpenter, J. K. & Kind, S. Effect of treatments for depression on quality of life: a meta-analysis. *Cogn. Behav. Ther.* **46**, 265–286 (2017).
5. Locher, C. et al. Efficacy and safety of selective serotonin reuptake inhibitors, serotonin-norepinephrine reuptake inhibitors, and placebo for common psychiatric disorders among children and adolescents: a systematic review and meta-analysis. *JAMA Psychiatry* **74**, 1011 (2017).
6. Haddad, P. The SSRI discontinuation syndrome. *J. Psychopharmacol.* **12**, 305–313 (1998).
7. Steinert, C., Hofmann, M., Kruse, J. & Leichsenring, F. Relapse rates after psychotherapy for depression – stable long-term effects? A meta-analysis. *J. Affect. Disord.* **168**, 107–118 (2014).
8. Nutt, D. & Carhart-Harris, R. The current status of psychedelics in psychiatry. *JAMA Psychiatry* <https://doi.org/10.1001/jamapsychiatry.2020.2171> (2020).
9. Lyons, T. & Carhart-Harris, R. L. More realistic forecasting of future life events after psilocybin for treatment-resistant depression. *Front. Psychol.* **9**, 1721 (2018).
10. Beck, A. T. & Clark, D. A. Anxiety and depression: an information processing perspective. *Anxiety Res.* **1**, 23–36 (1988).
11. Rolls, E. T. A non-reward attractor theory of depression. *Neurosci. Biobehav. Rev.* **68**, 47–58 (2016).
12. Hamilton, J. P. et al. Default-mode and task-positive network activity in major depressive disorder: implications for adaptive and maladaptive rumination. *Biol. Psychiatry* **70**, 327–333 (2011).
13. Kendler, K. S. The phenomenology of major depression and the representativeness and nature of DSM criteria. *Am. J. Psychiatry* **173**, 771–780 (2016).
14. Goodman, Z. et al. Whole-brain functional dynamics track depressive symptom severity. *Cereb. Cortex* <https://doi.org/10.1093/cercor/bhab047> (2021).
15. Margulies, D. S. et al. Situating the default-mode network along a principal gradient of macroscale cortical organization. *Proc. Natl Acad. Sci. USA* **113**, 12574–12579 (2016).
16. Andrews-Hanna, J. R., Smallwood, J. & Spreng, R. N. The default network and self-generated thought: component processes, dynamic control, and clinical relevance: the brain’s default network. *Ann. NY Acad. Sci.* **1316**, 29–52 (2014).
17. Lydon-Staley, D. M. et al. Repetitive negative thinking in daily life and functional connectivity among default mode, fronto-parietal, and salience networks. *Transl. Psychiatry* **9**, 234 (2019).
18. Daws, R. E. et al. Optimisation of brain states and behavioural strategies when learning complex tasks. Preprint at *bioRxiv* <https://doi.org/10.1101/2020.06.17.156570> (2021).
19. Kim, C., Cilles, S. E., Johnson, N. F. & Gold, B. T. Domain general and domain preferential brain regions associated with different types of task switching: a meta-analysis. *Hum. Brain Mapp.* **33**, 130–142 (2012).
20. Turnbull, A. et al. Reductions in task-positive neural systems occur with the passage of time and are associated with changes in ongoing thought. *Sci. Rep.* **10**, 9912 (2020).

21. Wilkinson, P. O. & Goodyer, I. M. Attention difficulties and mood-related ruminative response style in adolescents with unipolar depression. *J. Child Psychol. Psychiatry* <https://doi.org/10.1111/j.1469-7610.2006.01660.x> (2006).
22. Vollenweider, F. X., Vollenweider-Scherpenhuyzen, M. F. I., Bäbler, A., Vogel, H. & Hell, D. Psilocybin induces schizophrenia-like psychosis in humans via a serotonin-2 agonist action. *NeuroReport* **9**, 3897–3902 (1998).
23. Beliveau, V. et al. The structure of the serotonin system: a PET imaging study. *NeuroImage* **205**, 116240 (2020).
24. Andersen, K. A. A., Carhart-Harris, R., Nutt, D. J. & Erritzoe, D. Therapeutic effects of classic serotonergic psychedelics: a systematic review of modern-era clinical studies. *Acta Psychiatr. Scand.* **143**, 101–118 (2021).
25. Carhart-Harris, R. L. et al. Psilocybin for treatment-resistant depression: fMRI-measured brain mechanisms. *Sci. Rep.* **7**, 13187 (2017).
26. Carhart-Harris, R. L. et al. Trial of psilocybin versus escitalopram for depression. *N. Engl. J. Med.* **384**, 1402–1411 (2021).
27. Nutt, D., Erritzoe, D. & Carhart-Harris, R. Psychedelic psychiatry's brave new world. *Cell* **181**, 24–28 (2020).
28. Carhart-Harris, R. L. & Friston, K. J. REBUS and the anarchic brain: toward a unified model of the brain action of psychedelics. *Pharmacol. Rev.* **71**, 316–344 (2019).
29. Lord, L.-D. et al. Dynamical exploration of the repertoire of brain networks at rest is modulated by psilocybin. *NeuroImage* **199**, 127–142 (2019).
30. Luppi, A. I. et al. LSD alters dynamic integration and segregation in the human brain. *NeuroImage* **227**, 117653 (2021).
31. Carhart-Harris, R. L. et al. Neural correlates of the psychedelic state as determined by fMRI studies with psilocybin. *Proc. Natl Acad. Sci. USA* **109**, 2138–2143 (2012).
32. Fried, E. I. The 52 symptoms of major depression: lack of content overlap among seven common depression scales. *J. Affect. Disord.* **208**, 191–197 (2017).
33. Mattar, M. G., Cole, M. W., Thompson-Schill, S. L. & Bassett, D. S. A functional cartography of cognitive systems. *PLoS Comput. Biol.* **11**, e1004533 (2015).
34. Mucha, P. J., Richardson, T., Macon, K., Porter, M. A. & Onnela, J.-P. Community structure in time-dependent, multiscale, and multiplex networks. *Science* **328**, 876–878 (2010).
35. Barrett, F. S., Doss, M. K., Sepeda, N. D., Pekar, J. J. & Griffiths, R. R. Emotions and brain function are altered up to one month after a single high dose of psilocybin. *Sci. Rep.* **10**, 2214 (2020).
36. Pasquini, L., Palhano-Fontes, F. & Araujo, D. B. Subacute effects of the psychedelic ayahuasca on the salience and default mode networks. *J. Psychopharmacol.* **34**, 623–635 (2020).
37. Parkes, L., Satterthwaite, T. D. & Bassett, D. S. Towards precise resting-state fMRI biomarkers in psychiatry: synthesizing developments in transdiagnostic research, dimensional models of psychopathology, and normative neurodevelopment. *Curr. Opin. Neurobiol.* **65**, 120–128 (2020).
38. Ye, M. et al. Changes of functional brain networks in major depressive disorder: a graph theoretical analysis of resting-state fMRI. *PLoS ONE* **10**, e0133775 (2015).
39. Feurer, C. et al. Resting state functional connectivity correlates of rumination and worry in internalizing psychopathologies. *Depress. Anxiety* <https://doi.org/10.1002/da.23142> (2021).
40. Roseman, L. et al. Emotional breakthrough and psychedelics: validation of the emotional breakthrough inventory. *J. Psychopharmacol.* **33**, 1076–1087 (2019).
41. Watts, R., Day, C., Krzanowski, J., Nutt, D. & Carhart-Harris, R. Patients' accounts of increased 'connectedness' and 'acceptance' after psilocybin for treatment-resistant depression. *J. Humanist. Psychol.* **57**, 520–564 (2017).
42. Murphy-Beiner, A. & Soar, K. Ayahuasca's 'afterglow': improved mindfulness and cognitive flexibility in ayahuasca drinkers. *Psychopharmacol.* **237**, 1161–1169 (2020).
43. Zeifman, R. J. et al. Post-psychedelic reductions in experiential avoidance are associated with decreases in depression severity and suicidal ideation. *Front. Psychiatry* **11**, 782 (2020).
44. Carhart-Harris, R. L. & Nutt, D. J. Serotonin and brain function: a tale of two receptors. *J. Psychopharmacol.* **31**, 1091–1120 (2017).
45. Wang, X., Öngür, D., Auerbach, R. P. & Yao, S. Cognitive vulnerability to major depression: view from the intrinsic network and cross-network interactions. *Harv. Rev. Psychiatry* **24**, 188–201 (2016).
46. Hampshire, A. et al. Probing cortical and sub-cortical contributions to instruction-based learning: regional specialisation and global network dynamics. *NeuroImage* **192**, 88–100 (2019).
47. Soreq, E., Violante, I. R., Daws, R. E. & Hampshire, A. Neuroimaging evidence for a network sampling theory of individual differences in human intelligence test performance. *Nat. Commun.* **12**, 2072 (2021).
48. Watanabe, T. & Rees, G. Brain network dynamics in high-functioning individuals with autism. *Nat. Commun.* **8**, 16048 (2017).
49. Gu, B.-M. et al. Neural correlates of cognitive inflexibility during task-switching in obsessive-compulsive disorder. *Brain* **131**, 155–164 (2007).
50. Wei, M. et al. Abnormal dynamic community structure of the salience network in depression: abnormal salience network in depression. *J. Magn. Reson. Imaging* **45**, 1135–1143 (2017).
51. Carhart-Harris, R. L. et al. Can pragmatic research, real-world data and digital technologies aid the development of psychedelic medicine? *J. Psychopharmacol.* <https://doi.org/10.1177/02698811211008567> (2021).
52. Carhart-Harris, R. L. et al. Psychedelics and the essential importance of context. *J. Psychopharmacol.* **32**, 725–731 (2018).
53. Tagliazucchi, E. & Laufs, H. Decoding wakefulness levels from typical fMRI resting-state data reveals reliable drifts between wakefulness and sleep. *Neuron* **82**, 695–708 (2014).
54. Leonardi, N. & Van De Ville, D. On spurious and real fluctuations of dynamic functional connectivity during rest. *NeuroImage* **104**, 430–436 (2015).
55. Finc, K. et al. Dynamic reconfiguration of functional brain networks during working memory training. *Nat. Commun.* **11**, 2435 (2020).

Publisher's note Springer Nature remains neutral with regard to jurisdictional claims in published maps and institutional affiliations.

© The Author(s), under exclusive licence to Springer Nature America, Inc. 2022

Methods

Trial overviews. The trial designs (Fig. 1) and main clinical outcomes of the open-label³¹ (gtr.ukri.org: MR/J00460X/1) and DB-RCT³² (clinicaltrials.gov: NCT03429075) trials have been previously published. Both trials were conducted at the National Institute for Health Research Imperial Clinical Research Facility and received Imperial College London Sponsorship, NHS research and Imperial college Joint Research and Compliance Office ethical approval, Health Research Authority and Medicines and Healthcare products Regulatory Agency approval. This work was conducted under a UK Home Office Schedule 1 Drug Licence. All participants provided written informed consent. Participants were not financially compensated.

Participants. For both trials, eligibility required a general practitioner-confirmed diagnosis of unipolar MDD (16+ on the 21-item Hamilton Depression Rating scale). The open-label trial had the additional criteria of TRD, as defined by no improvement despite multiple courses of antidepressant medication (mean = 4.6 ± 2.6 past medications; range, 2–11)³⁹. Patients were asked whether they had previous experience of using psychedelics. In the open-label trial, 25% had previous experience. Similarly, in the DB-RCT, 31% of patients in the psilocybin arm and 24% in the escitalopram arm had previous experience.

Exclusion criteria were immediate family or personal history of psychosis, risky physical health condition (physician-assessed), history of serious suicide attempts, positive pregnancy test and MRI contraindications. The DB-RCT had the additional exclusion criteria of SSRI contraindications or previous escitalopram use. Of note, treatment resistance was neither an inclusion or exclusion criterion in the DB-RCT. All eligible patients undertook telephone screening interviews, provided written informed consent and their mental and physical medical histories were thoroughly evaluated.

Interventions. Nineteen patients with TRD were recruited to the open-label trial and attended a 1-d pre-treatment baseline session that included eyes-closed resting-state fMRI and clinical assessment (Fig. 1a). This was followed by two psilocybin therapy DDs, separated by 1 week. A low dose of psilocybin (10 mg) was orally ingested on DD1 and followed by a high dose (25 mg) on DD2. The follow-up fMRI and clinical assessment occurred 1 d after DD2. Patients attended an on-site clinical assessment at 1 week after DD2 and completed further clinical assessment electronically at 3 and 6 months. Of the 19 patients with TRD, 16 were retained (mean age, 42.75 years; s.d. = 10.15, 4 female) for the present analysis after 3 were excluded due to excessive fMRI head motion (Fig. 2a).

Of the 59 MDD patients recruited to the DB-RCT, a random number generator allocated 30 to the psilocybin arm and 29 to the escitalopram arm (Fig. 1b). The final imaging samples for this investigation were $n = 22$ for the psilocybin arm (mean age, 44.5 years, s.d. = 11.0, 8 female) and $n = 21$ for the escitalopram arm (mean age, 40.9 years, s.d. = 10.1, 6 female) (Fig. 2b). Patients attended a pretreatment baseline eyes-closed resting-state fMRI. DD1 consisted of either 25 mg psilocybin (psilocybin arm) or a presumed negligible 1 mg psilocybin (escitalopram arm) dose. All patients were informed that they would receive psilocybin but were blind to the dosage. DD2 occurred 3 weeks after DD1 and was a duplicate dosage. There was no dosage crossover. Beginning 1 d after DD1, patients took daily capsules for 6 weeks and 1 d in total. For both conditions, one capsule per day was ingested for the first 3 weeks and two thereafter. Capsule content was either inert placebo (microcrystalline cellulose in the psilocybin arm) or escitalopram in the escitalopram arm, 10 mg for the first 3 weeks and 2 × 10 mg (20 mg) total thereafter.

Measuring depression severity. BDI-1A scores were used to assess depression severity in both studies. This patient-rated measure captures a broader range of symptoms, with an additional focus on the cognitive features of depression, compared with other measures such as the QIDS-SR-16 (ref. 40). BDI was preregistered as a primary outcome measure in the open-label trial (gtr.ukri.org MR/J00460X/1) and was measured at baseline and 1 week, 3 months and 6 months after DD2. For the DB-RCT, BDI was measured at baseline and 2, 4 and 6 weeks after DD1. BDI was a secondary outcome measure for this DB-RCT (ClinicalTrials.gov NCT03429075) and was used here to test for a replication of the effects observed in the open-label trial.

MRI acquisition. Brain imaging was performed on a 3T Siemens Tim Trio at Invicor. Anatomical images were acquired using the Alzheimer's Disease Neuroimaging Initiative, Grand Opportunity (ADNI-GO³⁶) recommended MPRAGE parameters (1-mm isotropic voxels; TR, 2,300 ms; TE, 2.98 ms; 160 sagittal slices; 256 × 256 in-plane field of view; flip angle, 9 degrees; bandwidth, 240 Hz per pixel; GRAPPA acceleration, 2).

In both studies, eyes-closed resting-state fMRI data were collected with T2*-weighted echo-planar images with 3-mm isotropic voxels. In study 1, a 12-channel head coil was used to acquire 240 volumes in ~8 min: TR, 2,000 ms; TE, 31 ms; 36 axial slices; flip angle, 80 degrees; bandwidth, 2,298 Hz per pixel; and GRAPPA acceleration, 2). In study 2, a 32-channel head coil was used to acquire 480 volumes in ~10 min: TR, 1,250 ms; TE, 30 ms; 44 axial slices; flip angle, 70 degrees; bandwidth, 2,232 Hz per pixel; and GRAPPA acceleration, 2).

fMRI data preprocessing. Imaging data were preprocessed via a custom in-house pipeline composed of tools from the FMRIB Software Library³⁷, Analysis of Functional NeuroImages (AFNI)³⁸, Freesurfer³⁹ and Advanced Normalization Tools⁴⁰ packages. Patients were excluded if either fMRI scan contained >20% of volumes with a framewise displacement >0.5 mm.

Specifically, the following preprocessing stages were performed: (1) removal of the first three volumes; (2) de-spiking (3dDespike, AFNI); (3) slice time correction (3dTshift, AFNI); (4) motion correction (3dvolreg, AFNI) by registering each volume to the volume most similar, in the least-squares sense, to all others; (5) brain extraction (BET, FSL); (6) rigid body registration to anatomical scans (BBR, FSL); (7) nonlinear registration to the 2 mm Montreal Neurological Institute (MNI) brain (Symmetric Normalization, Advanced Normalization Tools); (8) scrubbing, using a framewise displacement threshold of 0.5 mm, scrubbed volumes were replaced with the mean of the neighboring volumes; (9) 6 mm full width at half maximum Gaussian spatial smoothing (3dBlurInMask, AFNI); (10) 0.01 to 0.08 Hz band-pass filtering (3dFourier, AFNI); (11) linear and quadratic de-trending (3dDetrend, AFNI) and (12) voxelwise nuisance regression with the six realignment motion regressors and three tissue signal regressors (Ventricles, Freesurfer, eroded in 2 mm space), draining veins (FSL's CSF minus Freesurfer's Ventricles, eroded in 1 mm space) and local white matter (WM) (FSL's WM minus Freesurfer's subcortical gray matter structures, eroded in 2 mm space). Regarding local WM regression, AFNI's 3dLocalstat was used to calculate the mean local WM time series for each voxel, using a 25-mm radius sphere centered on each voxel.

Functional connectivity. Following the preprocessing, a functional atlas was used to separate the cerebral cortex into 100 regions of interest (ROIs)⁶¹. FC between each pair of ROIs was calculated with a Pearson correlation coefficient between each pair of mean signal 'time courses' (representing fluctuations in neural activity over time). This resulted in an $N \times N$ FC matrix, with each element representing the connectivity strength between a pair of ROIs. Positive values were retained and Fisher-transformed to z scores. This procedure was repeated independently for each patient and scan (baseline and post-treatment).

Brain network modularity. The community structure or segregation between the brain's functional networks, was measured by summarizing each FC matrix with a common Louvain-like community detection algorithm⁶² where the objective is to maximize the extent to which brain areas can be separated into nonoverlapping communities or modules. The modularity quality function score, Q^{63} , tends to be high when the brain exhibits a high segregation between its functional networks (such as strong clusters of FC within brain networks/communities with weak FC to the rest of the brain).

This approach has been commonly applied to fMRI data to characterize how brain function adapts in a number of contexts⁵⁵. Here, modularity, Q^{63} , was defined in the standard way by:

$$Q = \frac{1}{2m} \sum_{ij} \left(A_{ij} - \gamma \frac{k_i k_j}{2m} \right) \delta(c_i, c_j), \quad (1)$$

where A_{ij} represents the weight of FC (correlation) between ROI i and j , γ is the structural resolution free parameter (set to 1) and $\frac{k_i k_j}{2m}$ is the expected null FC defined with $k_i = \sum_j A_{ij}$ as the total FC across all connections with ROI i , c_i is the community to which ROI i is assigned, $\delta(c_i, c_j)$ is the Kronecker δ function and equals 1 if ROI i and j belong to the same community and 0 otherwise⁶⁴ and $m = \frac{1}{2} \sum_{ij} A_{ij}$ is the total FC of the network.

To allow valid comparisons between patients and scans, the modularity scores were generated 100 times and the partition with the largest modularity score was normalized by the mean modularity generated from 100 randomly rewired (shuffled) FC matrices⁶⁵. This common procedure was applied to account for the nondeterministic and near-degenerate partitions (solutions with differing but similar optimality) generated by Louvain algorithms and to account for modularity scores relating to the total sum of FC within the network⁶⁶. This process was repeated independently for each patient and scan.

Functional cartography. The community detection procedure generates a community assignment to each ROI. We used these labels to determine the extent to which ROIs were recruited to the functional network that they typically 'belong to', as defined by healthy adults (such as DMN regions should reliably form communities with each other).

First, we created an allegiance matrix, P^{33} , which represented the probability that two regions i and j were assigned to the same community across the 100 iterations of the modularity algorithm, defined here as:

$$P_{ij} = \frac{1}{O} \sum_{o=1}^O a_{ij}^{k,o} \quad (2)$$

where $O = 100$ as the number of partitions. For each partition, $a_{ij}^{k,o}$ equals 1 if regions i and j belong to the same community.

Using the allegiance matrix, we then summarized how often ROIs either formed communities with ROIs from the same functional network (network recruitment) or formed communities with ROIs between different networks (between-network integration) across the partitions³³. These functional cartography measures were then normalized against the mean values from 1,000 randomly shuffled ROI network assignments to account for differences in the number of regions in each network³⁵. Finally, network recruitment and between-network integration scores were averaged at the network level using seven predefined cortical networks³⁴.

Dynamic flexibility. The short TR used in the fMRI protocol of study 2 generated approximately twice the number of time points, and this afforded an additional analysis of dynamic flexibility. Multilayer modularity estimation³⁴ was conducted using a $N \times N \times T$ matrix of 30 volume-sliding windows (37.5 s of real time) with 50% overlap. This window size is typical for estimating dynamic FC with fMRI³⁴. For each patient and scan, multilayer modularity, Q_{ML} , was estimated 100 times from each $N \times N \times T$ FC matrix by:

$$Q_{ML} = \frac{1}{2\mu} \sum_{ijl} \left[\left(A_{ijl} - \gamma_l \frac{k_{il}k_{jl}}{2m_l} \right) \delta_{lr} + \delta_{ij} \omega_{jlr} \right] \delta(c_{il}, c_{jr}), \quad (3)$$

where $\mu = \frac{1}{2} \sum_{ijl} A_{ijl}$ is the total FC of the multilayer network, and $m_l = \frac{1}{2} \sum_{ijl} A_{ijl}$ is the total FC of layer l , A_{ijl} is the FC between ROI i and j at layer l , $\frac{k_{il}k_{jl}}{2m_l}$ is the expected null FC at layer l . The two free γ and ω structural and temporal resolution parameters are used to scale the number of communities and strength of inter-layer edges, respectively. As is typical for fMRI modularity analyses, both were set to 1 (refs. ^{33,55}).

The multilayer modularity estimation generates an $N \times T$ matrix where each element represents the community assignment of each ROI at each layer (time window). From this, the flexibility metric, f , can be simply calculated as the number of times an ROI changes its community allegiance, given the number of observations⁵³:

$$f_i = 1 - \frac{1}{T-1} \sum_l^{T-1} \delta(c_{il}, c_{i,l+1}), \quad (4)$$

Flexibility scores close to 0 represent rigid ROIs whose community allegiance is stable across time, scores close to 1 represent flexible ROIs whose community allegiance regularly changes (highly flexible). Network level flexibility scores were defined by the average flexibility of ROIs assigned to the given network.

Reporting Summary. Further information on research design is available in the Nature Research Reporting Summary linked to this article.

Data availability

All requests for raw and analyzed data and materials are promptly reviewed by R.C.H. and D.J.N., chief investigator and principal investigator, respectively, on the original work. Patient-related data not included in the paper were generated as part of clinical trials and may be subject to patient confidentiality. Source data are provided with this paper.

Code availability

All analyses and data visualizations were conducted in MATLAB R2020a. Codes for generating each data figure are available at <https://github.com/rdaws/psilodep>.

References

56. Jack, C. R. et al. The Alzheimer's disease neuroimaging initiative (ADNI): MRI methods. *J. Magn. Reson. Imaging* **27**, 685–691 (2008).

57. Smith, S. M. et al. Advances in functional and structural MR image analysis and implementation as FSL. *NeuroImage* **23**, S208–S219 (2004).
58. Cox, R. W. AFNI: software for analysis and visualization of functional magnetic resonance neuroimages. *Comput. Biomed. Res.* **29**, 162–173 (1996).
59. Dale, A. M., Fischl, B. & Sereno, M. I. Cortical surface-based analysis. *NeuroImage* **9**, 179–194 (1999).
60. Avants, B. B., Tustison, N. & Song, G. Advanced normalization tools (ANTs). *Insight J.* **2**, 1–35 (2009).
61. Schaefer, A. et al. Local-global parcellation of the human cerebral cortex from intrinsic functional connectivity MRI. *Cereb. Cortex* **28**, 3095–3114 (2018).
62. Blondel, V. D., Guillaume, J.-L., Lambiotte, R. & Lefebvre, E. Fast unfolding of communities in large networks. *J. Stat. Mech. Theory Exp.* **2008**, P10008 (2008).
63. Newman, M. E. J. & Girvan, M. Finding and evaluating community structure in networks. *Phys. Rev. E* **69**, 026113 (2004).
64. Bassett, D. S. et al. Task-based core-periphery organization of human brain dynamics. *PLoS Comput. Biol.* **9**, e1003171 (2013).
65. Maslov, S. & Sneppen, K. Specificity and stability in topology of protein networks. *Science* **296**, 910–913 (2002).
66. Rubinov, M. & Sporns, O. Weight-conserving characterization of complex functional brain networks. *NeuroImage* **56**, 2068–2079 (2011).

Acknowledgements

R.E.D. was supported by an Engineering and Physical Sciences Research Council PhD scholarship at the Imperial College London Centre for Neurotechnology (EP/L016737/1). The research was carried out at the National Institute for Health Research/Wellcome Trust Imperial Clinical Research Facility. The open-label trial was funded by a Medical Research Council clinical development scheme grant (MR/J00460X/1). The DB-RCT was funded by a private donation from the Alexander Mosley Charitable Trust, supplemented by Founders of Imperial College London's Centre for Psychedelic Research.

Author contributions

This study was designed and planned by R.C.-H. and D.N. and conducted by B.G., M.B.W., D.E. and L.R. The specific analysis was designed by R.E.D. and C.T. The analysis was conducted and visualized by R.E.D. The manuscript was drafted by R.E.D., C.T. and R.C.-H. All authors contributed to the interpretation of the study results and revised and approved the manuscript for intellectual content. The corresponding author (R.E.D.) attests that all listed authors meet authorship criteria and that no others meeting the criteria have been omitted.

Competing interests

R.C.H. reports receiving consulting fees from Entheon Biomedical and Beckley Psytech; B.G. received consulting fees from SmallPharma; D.E. received consulting fees from Field Trip and Mydecine; D.N. received consulting fees from Algernon and H. Lundbeck and Beckley Psytech, advisory board fees from COMPASS Pathways and lecture fees from Takeda and Otsuka and Janssen plus owns stock in Alcarelle, Awakn and Psyched Wellness. The other authors declare no competing interests.

Additional information

Supplementary information The online version contains supplementary material available at <https://doi.org/10.1038/s41591-022-01744-z>.

Correspondence and requests for materials should be addressed to Richard E. Daws.

Peer review information *Nature Medicine* thanks David Hellerstein, Jared Van Snellenberg and the other, anonymous, reviewer(s) for their contribution to the peer review of this work. Primary Handling Editor: Jerome Staal, in collaboration with the *Nature Medicine* team.

Reprints and permissions information is available at www.nature.com/reprints.

Reporting Summary

Nature Research wishes to improve the reproducibility of the work that we publish. This form provides structure for consistency and transparency in reporting. For further information on Nature Research policies, see our [Editorial Policies](#) and the [Editorial Policy Checklist](#).

Statistics

For all statistical analyses, confirm that the following items are present in the figure legend, table legend, main text, or Methods section.

n/a Confirmed

- The exact sample size (n) for each experimental group/condition, given as a discrete number and unit of measurement
- A statement on whether measurements were taken from distinct samples or whether the same sample was measured repeatedly
- The statistical test(s) used AND whether they are one- or two-sided
Only common tests should be described solely by name; describe more complex techniques in the Methods section.
- A description of all covariates tested
- A description of any assumptions or corrections, such as tests of normality and adjustment for multiple comparisons
- A full description of the statistical parameters including central tendency (e.g. means) or other basic estimates (e.g. regression coefficient) AND variation (e.g. standard deviation) or associated estimates of uncertainty (e.g. confidence intervals)
- For null hypothesis testing, the test statistic (e.g. F , t , r) with confidence intervals, effect sizes, degrees of freedom and P value noted
Give P values as exact values whenever suitable.
- For Bayesian analysis, information on the choice of priors and Markov chain Monte Carlo settings
- For hierarchical and complex designs, identification of the appropriate level for tests and full reporting of outcomes
- Estimates of effect sizes (e.g. Cohen's d , Pearson's r), indicating how they were calculated

Our web collection on [statistics for biologists](#) contains articles on many of the points above.

Software and code

Policy information about [availability of computer code](#)

Data collection No software was used in data collection.

Data analysis fMRI data preprocessing was conducted using FSL, AFNI, Freesurfer abd ANTs, All analyses and data visualizations were conducted in Matlab R2020a. Code from the Brain Connectivity Toolbox (BCT) (brain-connectivity-toolbox.net) was used for the fMRI network analysis. All analysis and data visualization codes will be made available at <https://github.com/rdaws/psilodep>.

For manuscripts utilizing custom algorithms or software that are central to the research but not yet described in published literature, software must be made available to editors and reviewers. We strongly encourage code deposition in a community repository (e.g. GitHub). See the Nature Research [guidelines for submitting code & software](#) for further information.

Data

Policy information about [availability of data](#)

All manuscripts must include a [data availability statement](#). This statement should provide the following information, where applicable:

- Accession codes, unique identifiers, or web links for publicly available datasets
- A list of figures that have associated raw data
- A description of any restrictions on data availability

The data presented in each figure are available at <https://github.com/rdaws/psilodep>. The raw MRI data are available upon reasonable request to RCH.

Field-specific reporting

Please select the one below that is the best fit for your research. If you are not sure, read the appropriate sections before making your selection.

Life sciences Behavioural & social sciences Ecological, evolutionary & environmental sciences

For a reference copy of the document with all sections, see [nature.com/documents/nr-reporting-summary-flat.pdf](https://www.nature.com/documents/nr-reporting-summary-flat.pdf)

Life sciences study design

All studies must disclose on these points even when the disclosure is negative.

Sample size	<p>Study1: This feasibility open-label trial recruited 19 patients with treatment resistant unipolar depression. The sample size is due to the primary aims of feasibility and safety associated with this trial.</p> <p>Study2: This phase 2, double-blind, RCT recruited 59 patients with major unipolar depression. The sample size is was chosen to allow between trial-arm comparisons and was sufficient for detecting medium to large effect sizes.</p>
Data exclusions	<p>Study1: Three patients were excluded for excessive fMRI head-motion. This resulted in a final analytical sample of n=16.</p> <p>Study2: Of the 29 randomly assigned to the escitalopram-arm: 1 patient did not complete the follow-up due to Covid 19 UK 'lockdown', 4 patients discontinued the intervention due to adverse side effects and 3 patients were excluded due to excessive fMRI head-motion.</p> <p>Of the 30 randomly assigned to the psilocybin-arm, 2 patients did not complete follow-up due to Covid 19 Uk 'lockdown', 1 patient discontinued taking daily placebo tablets and 5 patients were excluded due to excessive fMRI head motion.</p> <p>Together, this resulted in a final analytical sample of n=21 in the escitalopram-arm and n=22 in the psilocybin-arm.</p>
Replication	<p>In both studies, psilocybin therapy was associated with significant decreases in brain network modularity.</p> <p>This robust replication was further bolstered by significant patient correlation analyses. In both studies, the reductions in modularity that followed psilocybin therapy correlated with long-term improvements in depression severity.</p> <p>Across studies, the secondary analyses of network-level cartography did not replicate; however, the inferences from each study converged on the same brain networks whose organisation changes in a consistent manner across studies. Moreover, the changes that followed psilocybin therapy were predicted by, and consistent with, previously reported functional abnormalities in depression. While consistent, these effects were observed with a 'static' approach in study 1 and with a 'dynamic' approach in study 2.</p> <p>The difference between trials may reflect significant differences in depression symptom severity, trial designs and/or fMRI acquisition parameters.</p>
Randomization	<p>Study1: All patients underwent the same protocol. No randomization was required for this open-label feasibility trial. All analyses depended on within-subject changes that followed the intervention. Supplemental analyses indicate that the findings are robust to confounding factors, including fMRI head-motion.</p> <p>Study2: A random number generator was used to randomly assign patients to the psilocybin-arm or escitalopram-arm.</p>
Blinding	<p>Study1: In this open-label trial, the dosage and compound were known to both the patients and investigators.</p> <p>Study2: In this double-blind RCT, the patients and investigators were blind to the trial-arm, psilocybin therapy dosage (a negligible 1mg vs 25mg) and daily capsule contents (escitalopram vs placebo). More specifically, patients in the psilocybin-arm received 2 x 25mg psilocybin therapy sessions and daily placebo tablets. Patients in the escitalopram-arm received 2 x 1mg psilocybin therapy sessions and daily escitalopram tablets.</p>

Reporting for specific materials, systems and methods

We require information from authors about some types of materials, experimental systems and methods used in many studies. Here, indicate whether each material, system or method listed is relevant to your study. If you are not sure if a list item applies to your research, read the appropriate section before selecting a response.

Materials & experimental systems

n/a	Involved in the study
<input checked="" type="checkbox"/>	<input type="checkbox"/> Antibodies
<input checked="" type="checkbox"/>	<input type="checkbox"/> Eukaryotic cell lines
<input checked="" type="checkbox"/>	<input type="checkbox"/> Palaeontology and archaeology
<input checked="" type="checkbox"/>	<input type="checkbox"/> Animals and other organisms
<input type="checkbox"/>	<input checked="" type="checkbox"/> Human research participants
<input type="checkbox"/>	<input checked="" type="checkbox"/> Clinical data
<input checked="" type="checkbox"/>	<input type="checkbox"/> Dual use research of concern

Methods

n/a	Involved in the study
<input checked="" type="checkbox"/>	<input type="checkbox"/> ChIP-seq
<input checked="" type="checkbox"/>	<input type="checkbox"/> Flow cytometry
<input type="checkbox"/>	<input checked="" type="checkbox"/> MRI-based neuroimaging

Human research participants

Policy information about [studies involving human research participants](#)

Population characteristics	<p>Study1: Mean age=42.75, SD=10.15, 4/16 female. Study2: Psilocybin-arm - Mean age 40.9, SD=10.1, 6/21 female. Escitalopram-arm - Mean age=44.5, SD =11.0, 8/22 female.</p> <p>For both trials, eligibility required a general practitioner (GP) confirmed diagnosis of unipolar major depressive disorder (MDD) (16+ on the 21-item Hamilton Depression Rating scale [HAM-D]). The open-label trial had the additional criteria of treatment-resistant depression, as no improvement despite multiple courses of antidepressant medication (mean = 4.6 ± 2.6 past medications, range = 2-11).</p>
Recruitment	<p>For both studies, exclusion criteria were: Immediate family or personal history of psychosis, risky physical health condition (physician-assessed), history of serious suicide attempts, positive pregnancy test and MRI contraindications. Study 2 had the additional exclusion criteria of selective serotonin reuptake inhibitor (SSRI) contraindications or previous escitalopram use. Eligible patients undertook telephone screening interviews, provided written informed consent and their mental and physical medical histories were thoroughly evaluated.</p> <p>It is possible that expectancy effects could have influenced the present results. For example, an approximate minority of 1/4 to 1/3 of patients reporting having prior experience of psychedelics.</p>
Ethics oversight	<p>Both studies were conducted at the NIHR Imperial Clinical Research Facility and received Imperial College London Sponsorship, NHS research and Imperial college Joint Research and Compliance Office (JRCO) ethical approval, Health Research Authority and MHRA approval. This work was done under a UK Home Office Schedule 1 Drug License.</p>

Note that full information on the approval of the study protocol must also be provided in the manuscript.

Clinical data

Policy information about [clinical studies](#)

All manuscripts should comply with the ICMJE [guidelines for publication of clinical research](#) and a completed [CONSORT checklist](#) must be included with all submissions.

Clinical trial registration	<p>Study1: UKRI MRC - MR/J00460X/1 Study2: Clinicaltrials.gov - NCT03429075</p>
Study protocol	<p>Study1: Carhart-Harris et al. (2016), doi:10.1016/S2215-0366(16)30065-7, gtr.ukri.org/projects?ref=MR%2FJ00460X%2F1 Study2: Carhart-Harris et al. (2021), doi:10.1056/NEJMoa2032994, clinicaltrials.gov/ct2/show/NCT03429075?term=NCT03429075&draw=2&rank=1</p>
Data collection	<p>For both studies, visits occurred at the NIHR Imperial Clinical Research Facility. Study1 recruitment and data collection: April-2015 to April-2016. Study2 recruitment and data collection: January-2019 to March-2020.</p>
Outcomes	<p>For both studies, Beck depression inventory (BDI) scores and resting-state fMRI global brain network modularity were the primary measures of interest. BDI was well-suited for testing the primary hypothesis due to its emphasis on the cognitive features of depression and it is a reliable index of broader subjective symptomatology - mappable to brain function.</p> <p>Brain network modularity is an elegant composite measure of the brain's functional community structure. Abnormally modular, or segregated, network organization has previously been observed in depression patients and this measure correlates with symptom severity. In contrast, the acute action of psilocybin promotes a global decrease in network modularity (high integration) in healthy adults. Moreover, psilocybin therapy has been seen to deliver rapid, substantial and sustained reductions in depression severity.</p> <p>Therefore, it was hypothesized that the efficacy of psilocybin therapy for depression is underpinned by a sub-acute 'carryover' effect, and predicted that this would be observed as a long-term reduction in depression severity that follows, and correlates with, a decrease in network modularity. Changes in fMRI network modularity scores between the baseline and follow-up scans were assessed with at the group-level with paired t-tests. Pearson correlation analyses were conducted between the changes in modularity and the BDI severity scores.</p> <p>The secondary analyses focused on network-level cartography. These analyses provided a deeper, finer-grained, understanding of the changes in brain function that follow psilocybin therapy. Network metrics were assessed at the group-level with paired t-tests and Pearson correlation analyses were conducted between the changes in network flexibility and the BDI severity scores.</p>

Magnetic resonance imaging

Experimental design

Design type	Resting-state blood oxygen level dependent fMRI (eyes closed)
Design specifications	<p>Study 1: Two rs-fMRI scans per subject, each with 240 measurements (TR=2000ms). Study 2: Two rs-fMRI scans per subject, each with 480 measurements (TR=1250ms).</p>

Behavioral performance measures

Acquisition

Imaging type(s) Field strength Sequence & imaging parameters Area of acquisition Diffusion MRI Used Not used

Preprocessing

Preprocessing software Normalization Normalization template Noise and artifact removal Volume censoring

Statistical modeling & inference

Model type and settings Effect(s) tested Specify type of analysis: Whole brain ROI-based Both

Anatomical location(s)

Statistic type for inference (See [Eklund et al. 2016](#)) Correction

Models & analysis

n/a Involved in the study Functional and/or effective connectivity Graph analysis Multivariate modeling or predictive analysis

Functional and/or effective connectivity

Pearson correlation was used to estimate functional connectivity. This was conducted between pair of ROIs to construct functional connectivity matrices for each subject and scanning session.

Graph analysis

Network modularity, and related measures, were estimated using a community detection algorithm applied to the positive functional connectivity weights. Measures were controlled for near-degeneracy and also normalized with a random reshuffling permutation approach. Modularity measures were estimated for each subject and scan before being compared at the group-level and in the individual differences analyses.